The CO2-binding capacity of synthetic anhydrous and hydrates: Validation of a test method based on the instantaneous reaction rate

Mouna Boumaaza, Bruno Huet, Philippe Turcry, Abdelkarim Aït-Mokhtar

▶ **To cite this version:**

Mouna Boumaaza, Bruno Huet, Philippe Turcry, Abdelkarim Aït-Mokhtar. The CO2-binding capacity of synthetic anhydrous and hydrates: Validation of a test method based on the instantaneous reaction rate. Cement and Concrete Research, 2020, 135, pp.106113 -. 10.1016/j.cemconres.2020.106113 . hal-03490152

HAL Id: hal-03490152
https://hal.science/hal-03490152v1

Submitted on 3 Jun 2022

HAL is a multi-disciplinary open access archive for the deposit and dissemination of scientific research documents, whether they are published or not. The documents may come from teaching and research institutions in France or abroad, or from public or private research centers.

L'archive ouverte pluridisciplinaire **HAL**, est destinée au dépôt et à la diffusion de documents scientifiques de niveau recherche, publiés ou non, émanant des établissements d'enseignement et de recherche français ou étrangers, des laboratoires publics ou privés.

Distributed under a Creative Commons Attribution - NonCommercial 4.0 International License

Version of Record: https://www.sciencedirect.com/science/article/pii/S0008884619314826
Manuscript_dcabf67594993905cd19ae132a60618b

The CO_2-binding capacity of synthetic anhydrous and hydrates: validation of a test method based on the instantaneous reaction rate

Mouna Boumaaza*[1,2,3], Bruno Huet[1], Philippe Turcry[2], Abdelkarim Aït-Mokhtar[2]

[1] *LafargeHolcim Innovation Center, 95 rue du Montmurier, F-38070 Saint Quentin Fallavier, France*

[2] *Laboratoire des Sciences de l'Ingénieur pour l'Environnement (LaSIE), UMR 7356 CNRS, Université de La Rochelle, Avenue Michel Crépeau, F-17042 La Rochelle, France*

[3] *Technische Universität München, cbm, Centrum Baustoffe und Materialprüfung Baumbachstraße 7, D-81245 München, Germany*

ABSTRACT

In the present work, a new experimental setup is designed and validated to characterize the CO_2-binding capacity of cementitious materials based on their instantaneous rate of CO_2 uptake. An experimental investigation is carried out on synthetized anhydrous (C_3S, C_2S, C_3A) and hydrates (CH, C-S-H, AFt) exposed to ambient CO_2 concentration at three different relative humidity (RH) levels. The BET surface area and the density are determined before and after exposure to natural carbonation. Results show that the CO_2- binding capacity and rate increases highly with the RH. The instantaneous binding rate of the materials ranges from 10^{-6} to 5.10^{-10} $g_{co2}.g_{powder}^{-1}.s^{-1}$. The highest degree of carbonation is found for ettringite powder (DoC=45%). C_2S and C_3A are only slightly carbonated (DoC=3%), while significant carbonation of C_3S is observed only at 93% RH (DoC=14%). A good (R^2=0.94) agreement between the results determined using the new test method and thermogravimetric analysis (TGA) is noticed.

Key words: CO_2-binding capacity; instantaneous binding rate; test method; hydrates; anhydrous

1 INTRODUCTION

Steel bars in reinforced concrete are protected from corrosion by means of a passivation layer, which forms at high pH values (>12). This high pH environment is obtained from the surrounding hydrated cement paste. However, once the atmospheric CO_2 manages to move through the concrete porous network, it dissolves in the pores' water, forming carbonate ions (CO_3^{2-}) that reacts with the reactive calcium content from the calcium-bearing phases in the cement [1][2]. This

© 2020 published by Elsevier. This manuscript is made available under the CC BY NC user license
https://creativecommons.org/licenses/by-nc/4.0/

reaction converts Ca^{2+} ions into calcium carbonate ($CaCO_3$). Carbonation is the term used to describe this physicochemical process.

The carbonation front is usually determined using a colorimetric method based on a pH indicator solution, such as phenolphthalein [3]. This method provides only an approximate measurement of the real carbonation depth in terms of pH values and does not give an estimation of the carbonation extent at any depth [4][5][6].

The carbonation depth and rate are controlled by the diffusion process of gaseous CO_2 and the CO_2-binding capacity [7], which is the quantity of CO_2 bound per mass of binder. Test methods that determine the gas diffusivity of cementitious materials can be found in the literature, e.g. [8][9][10][11]. Although gas diffusion is in many situations the slowest mechanism of the overall process [12], an accurate quantification of the CO_2-binding capacity is of critical importance for understanding and modeling the carbonation behavior of cementitious materials [13][14]. So far, to the authors' knowledge, there is no standardized test method that allows determining these two properties. To address this issue, it is very important to develop reliable, accurate, cost-effective and time-saving test methods to determine the gas transport property of cementitious materials and their CO_2-binding capacity and rate separately.

One way to evaluate the CO_2-binding capacity is applying the thermogravimetric analysis technique (TGA) to measure the weight loss resulting from the thermal decomposition of different phases in the cementitious materials. The temperature of decarbonation is defined separately for each mineral. Usually, the weight loss peak between 530°C to 950ºC is caused by the decomposition of $CaCO_3$ and the consequent release of CO_2 [15]. This technique is destructive, allows a rough quantification of the CO_2-binding capacity in an uncontinous way and gives an average value of its cumulative rate. TGA is sometimes coupled with XRD-Rietveld that helps quantifying the amounts of CO_2 bound in the crystalline phases only. Major limitations of these techniques are that the CO_2 contained in the amorphous carbonated pastes is not considered by XRD and the CO_2 mass loss due to some carbonates (e.g. $MgCO_3$) has a temperature range that may overlap the portlandite's and the bound water in the C-S-H gel pores in TGA results [16].

Fourier transform infrared spectroscopy (FTIR) is also shown to be a suitable technique to monitor the formation of carbonates in cement [17][18]. The latter relies on the vibration modes of characteristic groups in a compound, and not on the crystallinity of the sample [18].

Other techniques in the literature have been developed to examine the CO_2-binding capacity and rate. Van Balen et al. [19] developed an experimental setup to continuously measure the carbon dioxide uptake of lime samples. It consists of a closed loop in which a mixture of air and carbon dioxide (15-50% CO_2 concentration) is introduced at a certain RH (at 20°C). From the analysis of the CO_2 concentration vs. time, the uptake rate (derivative), maximum and average speed of carbon dioxide uptake are calculated. These authors found that the carbonation reaction is zeroth order within the CO_2 concentration range of their study (as also reported by Shih-Min Shih et al. [20]). A good reliability of the test method (10-20%) is reported, but the test method results do not agree with the TGA results.

El-Turki el al [21] developed a micro-balance technique to measure the mass variation of samples of mortars, cement and lime pastes during carbonation at 100% CO_2 concentration by volume and a RH between 65% and 97%. Analysis of the mass-variation data provides direct determination of the carbonation rates. However, using this method, it is challenging to distinguish between the mass change due to water vapor absorption and the mass gain due to carbonation. The weight gain technique induces a lot of errors for evaluating the carbonation extent [22].

Little information on the carbonation kinetics and mechanisms of the anhydrous and hydrates can be found in the research involving carbonation of cementitious materials. The present work seeks to address this gap through an investigation of the carbonation kinetics and mechanisms of the main hydrates (CH, AFt, and C-S-H) and anhydrous phases (C_3S, C_2S, and C_3A) present in concrete. First, a simple and affordable test method is developed and validated. This method allows determining the CO_2-binding capacity and rate of cementitious materials by monitoring their CO_2 uptake during the exposure to ambient CO_2 concentration in a RH and temperature-controlled environment. Direct measurements of carbon dioxide uptake should avoid possible errors using weight gain as a measure for the carbonation process, as has been shown by Aono [23]. A range of complementary analytical techniques, including thermogravimetric analysis (TGA), Brunauer-

Emmett-Teller (BET), density, and scanning electron microscopy (SEM) are used to help the further understanding of the carbonation behavior of the tested materials.

2 MATERIALS AND METHODS

2.1 Synthetic minerals preparation

In order to enhance the understanding of the carbonation kinetics of the anhydrous phases of cement paste, triclinic tricalcium silicate (C_3S), dicalcium silicate (β-C_2S) and cubic tricalcium aluminate (C_3A), which are the three main anhydrous phases present in the clinker, are prepared.

The synthesis of these pure materials was carried out following a modified Pechini process, as described in [24]. The advantage of this method is that pure β-C_2S can be formed with no stabilizing impurities. Phases are produced, respecting the stoichiometric amounts of the oxide components of the anhydrous phases. The heating temperature for C_3S, C_2S and C_3A are: 1600°C, 1550°C, and 1350°C, respectively. These materials are grinded and sieved to 63 µm.

The main hydrated phases present in Portland cement were also prepared: portlandite (CH), calcium silica hydrates (C-S-H), and ettringite (AFt). The synthesis of ettringite is achieved by mixing tricalcium aluminate and gypsum using a wet process and then dried at 50°C. Pure portlandite was prepared by calcite decarbonation at 1000°C, cooling it down to ambient temperature and adding water. Calcium silicate hydrate with a Ca/Si = 0.9 was synthesized using CaO obtained from the calcination of $Ca(OH)_2$ for 4h at 1100°C, SiO_2 comes from hydrophilic silica fume Aerosil 90®. The water-per-solid ratio was 49. The mix was agitated for a month and then the solid phases were separated from the solution by centrifugation for 2 min at 12000 rpm, to be finally oven dried at 45°C under vacuum. Note that the Ca/Si ratio of C-S-H usually ranges between 0.8 and 1.6 [25] .C-S-H with low Ca/Si ratio is typical of cement paste with mineral additions, such as blast furnace slag (BFS). The carbonation of the latter was less studied in literature than carbonation of OPC pastes. Our experiments were carried out with C-S-H with Ca/Si of 0.9 to provide some data for a better understanding of the carbonation of materials with BFS.

The quality of the synthesis was controlled by means of a qualitative XRD test. Even though the preparation of the materials was done in a CO_2-free environment using boiled water cooled down to ambient temperature, and all the synthesized minerals were stored in closed bottles inside a chamber under vacuum with soda lime, traces of calcite were present in the XRD results and were

quantified using the thermogravimetric analysis (TGA) technique. After preparation of the samples, their density was measured using the helium pycnometer technique. The initial densities were found to agree with the results found by Balonis et al. [26]. The carbonation reactions of the studied phases are recalled in Table 1.

Cement phase	Reaction with CO_2
C_3S	$Ca_3SiO_5 + y\ H_2O + (3-x)CO_2 \rightarrow (CaO)_xSiO_2(H_2O)_y + (3-x)\ CaCO_3$
C_2S	$Ca_2SiO_4 + y\ H_2O + (2-x)CO_2 \rightarrow (CaO)xSiO_2(H_2O)y + (2-x)\ CaCO_3$
C_3A	$Ca_3Al_2O_6 + 6H_2O + 3CO_2 \rightarrow 3CaCO_3 + 2Al(OH)_3 + 3H_2O$
CH	$Ca(OH)_2 + CO_2 \rightarrow CaCO_3 + H_2O$
C-S-H	$(CaO)_x(SiO_2)_y(H_2O)_z + (x-x')CO_2 \rightarrow (CaO)_{x'}(SiO_2)_yH_{z'} + (x-x')CaCO_3 + (z-z')H_2O$
AFt	$3CaO.Al_2O_3.3CaSO_4.32H_2O + 3CO_2 \rightarrow 3\ CaCO_3 + Al_2O_3.xH_2O + 3CaSO_4.2H_2O + (26-x)H_2O$

Table 1: Carbonation reactions of the main cement phases [27][28][12][29]

It is worth noting that the presence of dissolved CO_2 may affect the stability of ettringite. In the previous work of Plank et al [30], it has been shown that ettringite is rather stable on air at ambient temperature, but it quickly decomposes under pressurized CO_2.

2.2 *Solid analysis*

A Brunauer–Emmett–Teller (BET) measurement was conducted on all the tested samples before and after the CO_2-binding capacity test. This technique uses an inert gas that does not react with the materials surfaces as an adsorbate to quantify the specific surface area [31]. In our case, the sample was first outgassed in a vacuum oven at 0.04 atm and 45°C.

The density of the tested samples is measured applying the helium pycnometer method [32] using the ACCUPYC 2 1340 MICROMERITICS pycnometer. A powdered specimen of about 5 g was compacted and placed inside a cell of a known volume pressurized with helium.

TGA tests were conducted in order to determine the bound CO_2 caused by the preparation of the samples before we began our tests, and the overall CO_2 binding capacity of the material afterwards. The TGA measurements were made under nitrogen flow at a heating rate of 10°C/min until 1000°C using a powdered sample of around 30 mg sieved at 63 µm.

The amount of bound CO_2 is calculated based on Equation 1, where m_{CO2} is the mass of CO_2 present in the sample and given by the TGA results, m_0 corresponds to the mass of the sample at 1000˚C.

$$CBC = \frac{m_{CO2}}{m_0}$$ Equation 1

The XRD technique was mainly used after the synthesis of the materials to evaluate their purity qualitatively and investigate the type of carbonates formed upon carbonation. Around 1 g of the powdered material (sieved at 63 µm), was introduced in a Philips/PANalytical X'Pert Pro-MPD diffractometer with an X'Celerator detector of an incident CuKα radiation beam by 40 kV and 40 mA to a rotation sample. The specimens were scanned for 40 minutes from 2θ = 5 to 65° by a step of 0.25° without protection from air CO_2 and in a dry environment (RH~40%).

Parallel to these experiments, scanning electron microscopy SEM [33] technique was used in order to observe the morphological changes in some powders upon carbonation. The powders were placed on a carbon adhesive sample holder and coated using gold-palladium as conductive material. The observations were made with a MEB-FEG FEI Quanta 400 device in the secondary electrons mode at an accelerated voltage of 15 KeV.

2.3 *Carbonation exposure conditions and equipment*

In order to perform a CO_2-binding capacity test, 1 g of the tested powder (with a maximum grain diameter of 63 □m) was evenly and thinly distributed over a PVC sample holder (Figure 1 (a)) of 110 mm diameter for exposure in the carbonation chamber in a room at 20 ± 2°C (Figure 1 (b)). The thickness of the powder sample on the holder is estimated to be lower than 63 µm, i.e. around the maximum grain diameter. Thus, each grain is assumed to be exposed to CO_2 what makes the homogeneization of the powder not necessary during the test. The RH inside the climate chamber was controlled by means of saturated salt solutions. The saturated salt solutions used to equilibrate the relative humidity inside the chambers are: 33% ($MgCl_2$), 55% ($Mg(NO3)_2$), 93% (KNO_3). The relative humidity level and the CO_2 concentration were monitored by means of sensors placed inside the chambers.

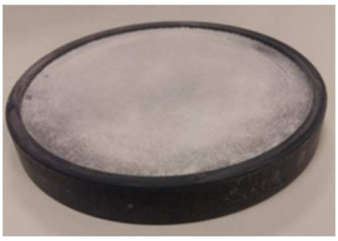

(a)

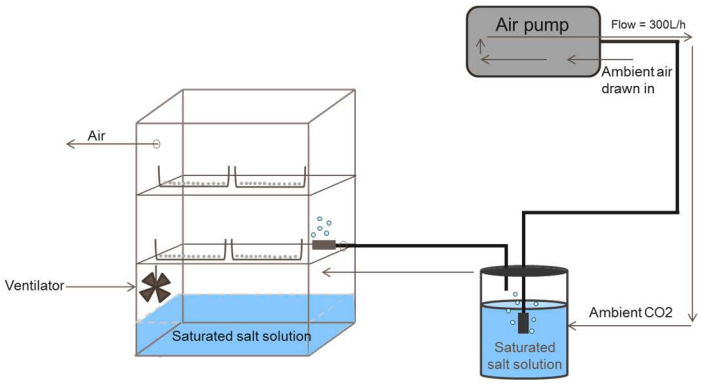

(b)

Figure 1: (a) A tested powder sample on the sample holder; (b) climate chamber during the natural carbonation of the powder specimen

In order to maintain the CO_2 concentration constant inside the climate chamber, an air pump of 300L/h flow rate was used to pass the ambient air through a bubbler filled with a saturated salt solution to regulate it at a certain RH and circulate it inside the climate chamber. This way, the RH, temperature and CO_2 concentration (450 ± 100 ppm) were kept constant inside the climate chamber. The volume of the chamber (40L) was well-ventilated thanks to a ventilator that ensured homogenization of the humid air at ambient CO_2 concentration.

2.4 *Instantaneous rate measurements*

2.4.1 Principle and apparatus

A new experimental device able to directly determine the CO_2 uptake of powdered samples was designed. The principle is to place over a short time interval a given mass of reactive powder in a closed cell where the initial CO_2 concentration is known. During this short period, the CO_2 depletion in the gas phase due to the uptake by the powder is measured by a sensor inside the cell. During all a carbonation period (1 month), the instantaneous CO_2 uptake is measured occasionally in the closed cell. For this purpose, the sample holder containing the powdered material (Figure 1 (a)) is

put inside the cell shown in Figure 2. After the CO_2 uptake measurement which lasts less than 30 min, the sample is returned in the climate chamber. The frequency of the CO_2 uptake measurements is twice a day for the first three days of carbonation and once a day afterwards.

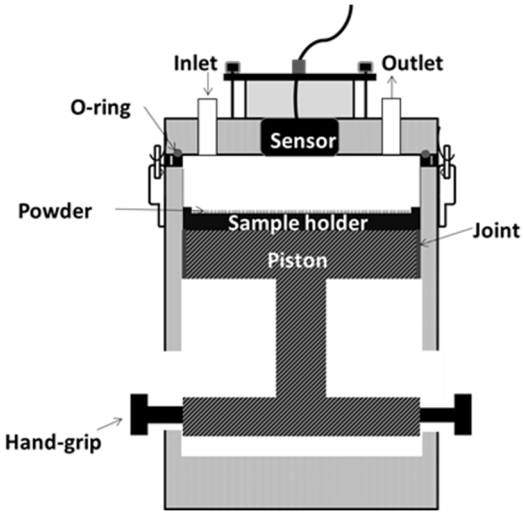

(a)

(b)

Figure 2 : Sketch (a) and photo (b) of the carbonation cell

The cell is a cylinder having an outside and inside diameter of 140 mm and 120 mm, respectively. The cell cover incorporates the infrared IR CO_2 gas sensor. An O-ring with a round cross-section is placed around the cover in order to seal the interface between the cover and the cell body. The cell closure is done manually by means of four stainless steel lockable clips. The total measurement

time of the CO_2 uptake by the sample must be negligible with regards to the overall carbonation period. Therefore, the cell body contains a 140 mm diameter piston of an adjustable height to vary the inside volume of the chamber. The latter can vary from 10 to 285 mL. The tests were carried out at ambient temperature (20°C) and pressure (1 atm). Note also that the carbonation cell is placed inside a climate chamber in order to regulate the relative humidity before introducing the sample holder and measuring the CO_2 uptake of the tested powder. However, during the measurement, the RH is not controlled inside the cell. It is assumed that the RH does not change during this period because of its brevity.

2.4.2 Analysis of the rates (from experimental data)

The collected experimental data are CO_2 depletion curves in the cell described previously over the carbonation exposure period. Figure 3 gives examples of CO_2 depletion in the gas phase over time in the case of ettringite powder after 1, 5 and 30 days of exposure to ambient CO_2 concentration in a climate chamber regulated at 93% RH. CO_2 depletion in the gas correspond to CO_2 uptake by the solid: we refer only to CO_2 uptake curves later in the document. The measurement period was around 30 min long. Each curve allows defining a rate of carbon dioxide uptake, which is proportional to its initial slope. It is noticed from Figure 3 that ettringite's reaction rate decreases as the carbonation reaction proceeds to drop sharply after 30 days of carbonation when the detection limit is reached.

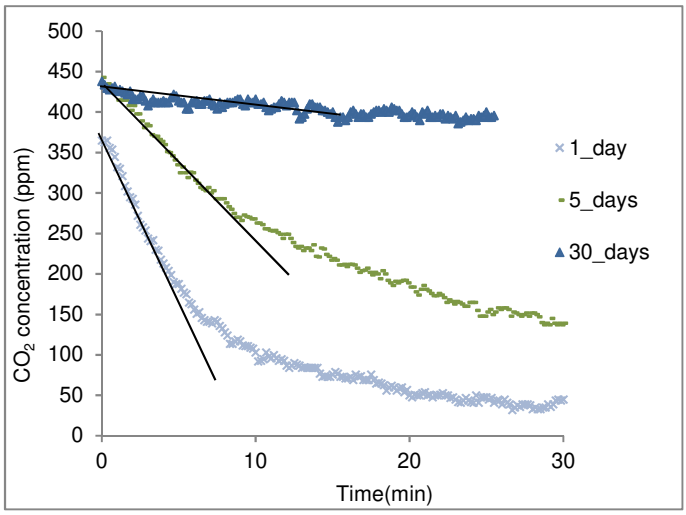

Figure 3: CO_2-uptake curves of ettringite powder at different carbonation periods: 1 day (gas volume = 123 mL), 5 and 30 days (gas volume = 10 mL)

By considering the CO_2-uptake curves, the instantaneous binding rate (*IBR*), the bound-CO_2 ($B_{\_CO2}$), and the degree of carbonation (*DoC*) are determined.

First, the initial slope (*S*) of each CO_2-uptake curve was determined automatically by maximizing the R-squared and minimizing the mean squared error using a statistical software (JMP). This slope is given in ppm.s^{-1} where ppm are moles mol CO_2/mol air.

The instantaneous binding rate is then calculated according to Equation 2, where *IBR* (g_{CO2} g^{-1}_{powder} s^{-1}) is the instantaneous CO_2-binding rate, *S* (ppm.s^{-1}) is the CO_2-uptake initial slope, *P* (Pa) the ambient pressure, *R* (m^3·Pa·K^{-1}·mol^{-1}) the ideal gas constant, *T* (K) the ambient temperature, V_g (m^3) the inside volume of the carbonation cell, M_{CO2} (g) the molar mass of carbon dioxide, and m_0 (g) is the mass of the material with neither unbound CO_2 nor water. This mass was calculated from the mass of the tested powder corrected by the mass loss results from TGA before carbonation of the sample (at 1000°C).

$$IBR = \frac{S * P * M_{CO2} * Vg}{R * T * m_0} \quad \text{Equation 2}$$

$$B_{\_CO2} = \int_{t=0}^{T} IBR\, dt \quad \text{Equation 3}$$

$$DoC = \frac{CBC}{MBC} \quad \text{Equation 4}$$

$$MBC = \sum \%CaO * \frac{M_{CO2}}{M_{CaO}} - \%SO3 * \frac{M_{CO2}}{M_{SO3}} \quad \text{Equation 5}$$

The bound-CO_2 ($B_{\_CO2}$) is deduced from the *IBR* by the trapezoidal integration of the *IBR* values between two CO_2-uptake measurements (from t=0 to *T* the time of the CO_2 uptake measurement) (Equation 3). The total CO_2-binding capacity (*CBC*) of the tested powder is the maximum value of the $B_{\_CO2}$ at the end of the carbonation period.

Note that the $B_{\_CO2}$ is expressed as the mass of CO_2 bound per mass of the powder (m_0). The degree of carbonation is calculated following Equation 4, where the maximum binding capacity (*MBC*) is calculated from the chemical composition of the tested material assuming that all CaO will be transformed into $CaCO_3$ except the one that reacts with SO_3 to form $CaSO_4$. The oxides

molar ratio is given from the stoichiometry of the chemical formulas of each synthesized material. M_{SO3}, M_{CO2}, M_{CaO} (g/mol) are the molar masses of trioxide sulfur, carbon dioxide and calcium oxide, respectively.

2.4.3 Analysis of the reaction order

The analysis of the CO_2-uptake curves determined using our experimental setup allows for the determination of the reaction order and the rate constant k_i (see Equations 6, 7 and 8). The analysis of the reaction order is of relevance regarding the measured instantaneous binding rates (see Equation 2) that are corrected according to the reaction rate.

The order of the reaction was determined by analyzing the slope of the linear graph obtained, whether with $[CO_2]$, ln ($[CO_2]$) or 1/$[CO_2]$, versus time and the linear fit quality (R-squared).

Zero order	$[CO_2](t) = -k_0 * t + [CO_2]_0$	Equation 6
First order	$\ln([CO_2](t)) = -k_1 * t + \ln([CO_2]_0)$	Equation 7
Second order	$\frac{1}{[CO_2](t)} = -k_2 * t + \frac{1}{[CO_2]_0}$	Equation 8

The order of reaction of a reactant indicates how much the rate of reaction changes if the concentration of the reactant is changed. The CO_2 concentration has no effect on the reaction rate of zeroth order reactions, while for first-order reactions, the rate of reaction changes directly with the concentration of the corresponding reactant. For second-order reactions, the rate of reaction changes as the square of the reactant concentration.

2.4.4 Test method and detection limit

In this work, six carbonation cells were used in parallel. Cells leakage rates were determined by performing blank tests: the cells were first flushed with nitrogen (from the inlet as shown on Figure 1), then the CO_2 concentration inside the cell was measured for 48 hours. Note that the blank tests were performed on all the cells at their maximum (285 mL) and minimum (10 mL) volumes. The collected data (CO_2 concentration vs. over time) were analyzed to calculate an equivalent CO_2-binding rate that sets the lower detection limit of the test method. Figure 4 (a) gives an example of leakage tests on a given cell (cell3). The minimum *IBR* that can be measured using our

experimental setup depends on the mass of the tested powder. Figure 4 (b) shows the decrease of the minimum *IBR* with the mass of the sample. However, experiments are conducted using 1 g of the powder in order to minimize the thickness of the grains layer and thus avoid mass diffusion during the carbonation exposure time. Therefore, the detection limit of the cell taken as an example is set at 5.8×10^{-10} $g_{CO2}.g_{powder}^{-1}.s^{-1}$.

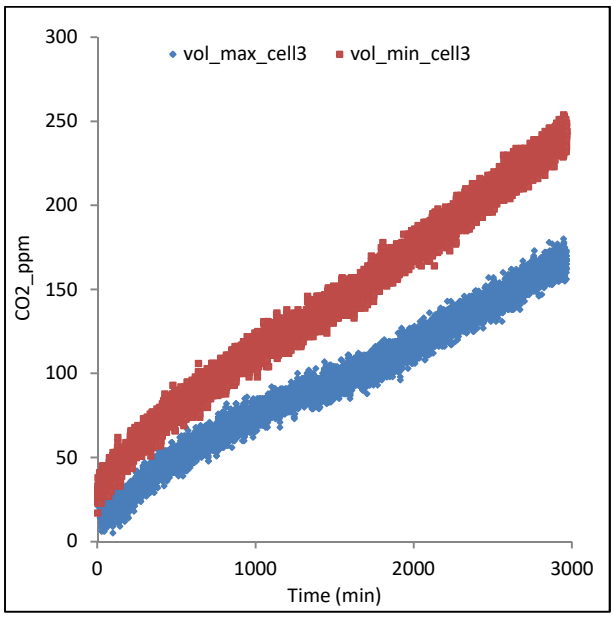

(a)

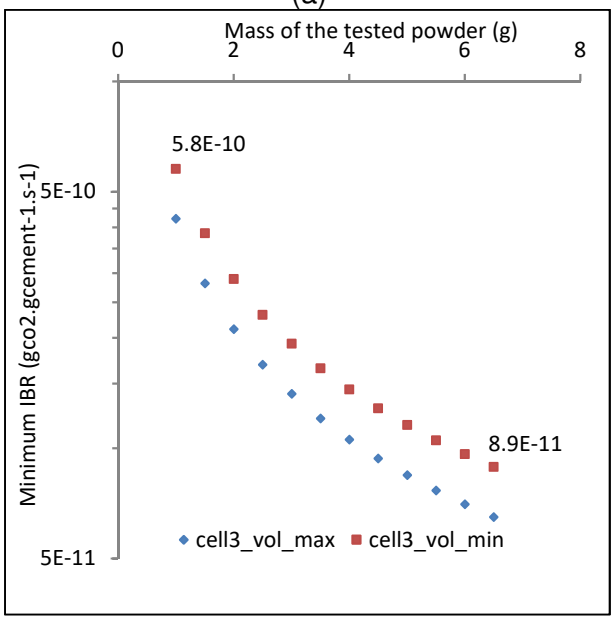

(b)

Figure 4: (a) example of a leakage test performed on a closed cell (cell3), (b) the minimum IBR that can be detected as a function of the sample mass

Note that the highest IBR (1.1×10^{-6} $g_{CO2}.g_{powder}^{-1}.s^{-1}$) determined with our test method corresponds to the value of the most reactive material (portlandite powder) tested during the first day of exposure to carbonation at the highest RH (93%).

3 Results

3.1 TGA and XRD results

3.1.1 TGA results of the materials after carbonation at 93% RH

Figure 5 shows an example of TGA results of the tested powders after carbonation at 93% RH. The TGA results are shown after carbonation at this RH only because the highest degree of carbonation is obtained at 93% RH. A peak is observed from 550°C to 950°C after carbonation of the materials. This result corresponds well to the temperature range of the decomposition of calcium carbonate reported in the literature [15]. Note that the interval between 550°C and 950°C is composed of multiple peaks for C-S-H and C_2S whereas a single peakfor CH. The composed peaks could be due to the overlapping of the thermal decomposition temperature of different phases [15]. After carbonation of C_2S and C_3S at 93% RH, TGA results show a certain amount of bound water (temperature range [150-250°C]), which could be due to the formation of C-S-H during the preconditioning with soda lime in the climate chamber prior the carbonation tests.

The TGA results of carbonated ettringite and C_3A show a peak around 280-300°C, which corresponds to the decomposition of aluminum hydroxide and/or Katoite. According to Collier [15], the thermal decomposition of aluminum hydroxide occurs within the same temperature range, and the thermal decomposition of katoite occurs between 200-250°C [28].

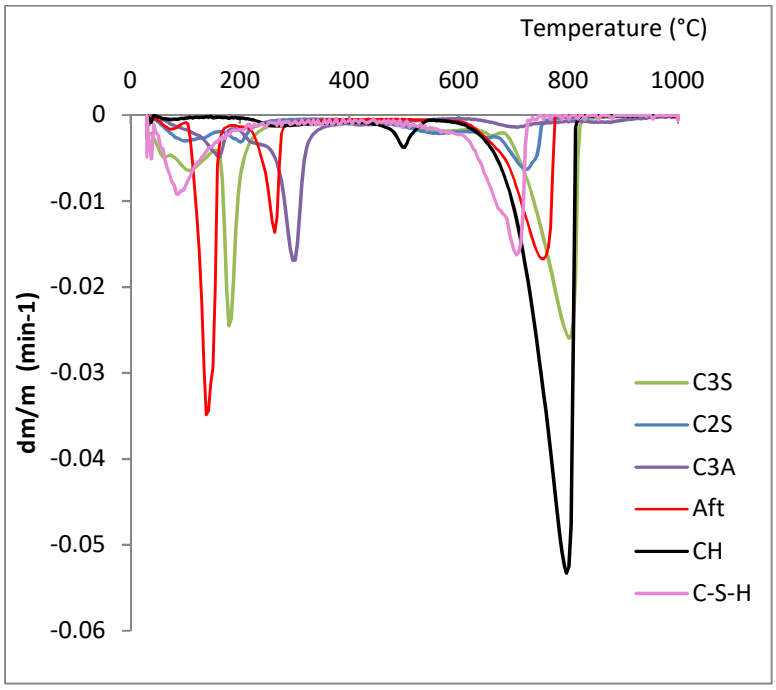

Figure 5: TGA results of C_3S, C_2S, C_3A, AFt, CH and C-S-H after carbonation at 93% RH

3.1.2 CO_2-binding capacity of the tested materials

The bound-CO_2 of the synthetic materials was determined using TGA, just before the conditioning at different RH levels with soda lime. Table 2 (column TGA initial in 10^{-2} g_{CO2} g^{-1}_{powder}) shows that some carbonation of the powdered samples could not be avoided, even if great care was taken to fill the climate chamber with soda lime (the CO_2 concentration inside the chamber was found to be less than 10 ppm). The maximum initial bound CO_2 is reached for portlandite powder (4.1 * 10^{-2} g_{CO2} g^{-1}_{powder} , DoC = 6.8%).

The bound CO_2 was also determined by TGA at the end of the carbonation period corresponding to the durations given in Table 2. Note that the initial bound CO_2 is deduced from these results. The CO_2-binding capacity of all the systems under all conditions is determined using Equation 1. Table 2 shows that the CO_2-binding capacity of all materials increases with the RH of exposure. The degree of carbonation varies between 1% and 45%, which highlights the incomplete carbonation of the materials, inspite of the very low rate at the end of the ageing period.

Material	Theoretical maximum binding capacity 10^{-2} g_{CO2} g^{-1}_{powder}	$B_{\_CO2}$ in 10^{-2} g_{CO2} g^{-1}_{powder} before the carbonation test (degree of carbonation)	RH (%)	CO_2 (ppm)	Ageing period (days)	$B_{\_CO2}$ in 10^{-2} $g_{CO2}.g^{-1}_{powder}$ after the carbonation test (degree of carbonation)
CH	59.5	4.1 (7%)	93	~450	14	23 (39%)
			55	~450	15	13.8 (23%)
			33	~450	25	7.0 (12%)
C-S-H	35.9	2.9 (8%)	93	~450	27	11.0 (31%)
			55	~450	27	5.4 (15%)
			33	~450	27	2.2 (6%)
Ettringite	38.9	2.1 (5%)	93	~450	35	17.6 (45%)
			55	~450	11	3.5 (9%)
			33	~450	29	1.5 (4%)
C_2S	51.2	0.1 (0.1%)	93	~10	32	0.5 (1%)
				~450	13	1.5 (3%)
			55	~450	13	0.8 (2%)
			33	~450	13	0.4 (1%)
C_3S	57.9	0.1 (0.1%)	93	~10	32	2.1 (1.2%)
				~450	14	8.0 (14%)
			55	~450	14	3.2 (6%)
			33	~450	15	0.6 (1%)
C_3A	48.9	0.6 (1.2%)	93	~10	32	1 (2.1%)
				~450	13	1.5 (3%)
			55	~450	13	1 (2%)
			33	~450	13	0.3 (1%)

Table 2: $B_{\_CO2}$ before and after the carbonation test at three RH levels: TGA results

In order to investigate the possible carbonation and hydrate formation by anhydrous materials during the preconditioning at 33%, 55% and 93% RH, the powders were stored inside climate chambers regulated at these RH for 32 days. Soda lime was added inside the climate chamber to avoid carbonation during this preconditioning period (CO_2=10ppm). The TGA raw data reveal only two peaks: [100-250°C] and [550-950°C]. The first corresponds to bound water, which could be a result of the formation of C-S-H for C_3S and C_2S, and the formation of aluminum hydroxide for C_3A powders [15]. Table 2 shows that the degree of carbonation after the preconditioning without soda lime of anhydrous minerals at 93% RH varies between 0.1% and 1.2%.

3.1.3 XRD results

XRD tests were carried out before the exposure of the materials to carbonation, after carbonation at 93% RH, and also after preconditioning of the anhydrous powders (C_3S, C_2S and C_3A) at 93%RH with soda lime for 32 days (CO_2 = 10 ppm) in order to investigate any possible formation of hydrates. Note that only the 93% RH exposure was tested for anhydrous minerals preconditioned without CO_2 and all materials carbonated at 93% RH, since the amount of bound CO_2 was the highest at this RH level. Indeed, Flatt et al. [34] suggest that alite stops hydrating below 80% RH. Qualitative XRD results are summarized in Table 3. All the powders did not carbonate fully, since a trace of the pure mineral in the powder is confirmed by XRD results (Table 3).

Material	State	Calcite	Aragonite	Vaterite	Gypsum	C_3S	AFt	CH	C_2S	C_3A
CH	After carbonation at 93%RH	++	-	-	-	-	-	+	-	-
C-S-H		++	+	+	-	-	-	-	-	-
AFt		+	++	-	++	-	+	-	-	-
C_3S		++	-	+	-	++	-	-	-	-
C_2S		+	-	-	-	-	-	-	++	-
C_3A		+	-	-	-	-	-	-		++

C_2S	After conditioning at 93%RH with soda lime.	-	-	-	-	-	-	-	++	
C_3S		-	-	-	-	++	-	-	-	-
C_3A		-	-	-	-	-	-	-	-	++

Table 3: results of qualitative XRD on synthetic materials after carbonation at 93% RH (++: phase highly present, +: phase present in lower quantity, -: phase not detected)

Results show that the only carbonate formed after the carbonation period of pure portlandite is calcite, which agrees with several findings in the literature [35][36]. Calcite is also the primary polymorph produced during the carbonation of C-S-H coexisting with small amounts of aragonite and vaterite, which could be linked to the Ca/Si ratio of the tested C-S-H (0.9). Indeed, Black et al. [37][38] studied the carbonation of synthetic C-S-H in which the initial Ca/Si ratio appeared to influence the crystalline carbonate species formed. For Ca/Si ratios greater than 0.67, principally calcite and vaterite were observed, whereas for ratios below 0.50, aragonite was most prevalent.

Ettringite carbonation is expected to form gypsum and amorphous aluminum hydroxide [39], which were not detected by XRD analysis (Table 3). However, the TGA results in Figure 5 for carbonated ettringite at 93% RH show a peak around 280-300°C, which corresponds to the decomposition of aluminum hydroxide according to Collier [15]. In agreement with our results, Nishikawa [29] and Zhou [40] reported that the carbonation of synthetic ettringite is accompanied by increasing formation of vaterite or aragonite, alumina gel and gypsum. However, Zhou and Glasser [40] observed only vaterite as the carbonate product formed, while Nishikawa et al. [29] described vaterite forming initially but aragonite being predominant at later stages.

The XRD analysis of the carbonated C_3S powder shows the formation of calcite as the main carbonation product with a trace of vaterite, while the analysis of the C_3A and β-C_2S powders after 14 days of natural carbonation at 93% RH only revealed small traces of calcite.

The XRD analysis of the C_3A and β-C_2S powders after 14 days of natural carbonation at 93% RH only revealed small traces of calcite. This result is due to the small $B_{\_CO2}$ of β-C_2S and C_3A and could be also a consequence of the formation of an amorphous calcium silicate hydrocarbonate

phase that is also shown by several researchers [41][42][43]. It is worth noting that no calcium hydroxide is detected by the XRD analysis after carbonation of C_3S. XRD results show no trace of calcite even though the degree of carbonation of anhydrous materials reached up to 1.2% (cf. Table 2). This could be explained by the formation of amorphous calcium carbonate. Indeed, in the previous work of Ashraf et al [44], it has been observed that during the carbonation of C_3S and C_2S, higher proportions of metastable $CaCO_3$ polymorphs are formed (i.e., aragonite, vaterite, and amorphous calcium carbonate (ACC)).

Research conducted by Seishi et al. [41] on the morphology of the carbonates formed after the reaction of pure C_3S with 5% CO_2 concentration under saturated humidity at room temperature revealed that calcite was the main product, coexisting with vaterite and aragonite. However, aragonite is recognized as the main carbonate for β-C_2S coexisting with traces of calcite and vaterite. Our differing results may be due to the fact that CO_2 concentrations differ. Han et al. [45] showed that C_3S and C_2S carbonation reaction results in the formation of $CaCO_3$ and silica gel.

3.2 Microstructure results (BET, SEM)

The BET surface area and density of anhydrous minerals CH and ettringite were determined before the beginning of the carbonation test and after carbonation at the three levels of RH. Figure 6 (b) shows that the BET surface area increased by a maximum factor of 1.7 when the anhydrous minerals and ettringite are carbonated at 33% and 55% RH, while it increased significantly (by a factor of 7) when these materials are carbonated at 93% RH. Nevertheless, for portlandite powder, the BET surface area decreases with the RH under which the carbonation test was carried out (by a factor of 6 at 93% RH). Regarding the density variation upon carbonation (Figure 6 (a)), an opposite trend is noticed: the density of the anhydrous phases decreased with the RH (by almost 1g/cm$^{3)}$ and the density of portlandite and ettringite increased significantly with the RH of carbonation. The BET surface area of C-S-H powder was only tested after carbonation at 93% RH and the density was not determined for practical reasons. A high decrease in the BET surface area was noticed on this powder (from 190 m²/g to 88 m²/g), which could be due to the precipitation of carbonates on the surface of the grains.

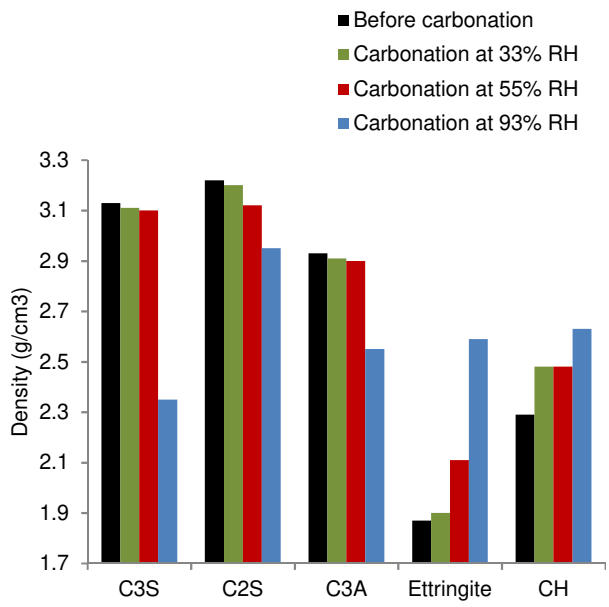

(a)

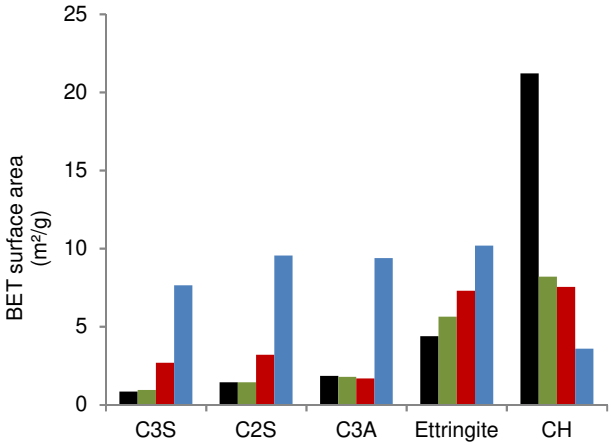

(b)

Figure 6 : The density (a) and BET surface area (b) of the materials before and after carbonation at different RH

Figure 7 shows the SEM images of C_3S, CH and AFt before carbonation and after carbonation at 93% RH. These images allow for the observation of the morphological evolution of the grains upon carbonation. Figure 7 (b) and (d) show an increase in the amount of carbonation products on the surface of C_3S and CH after carbonation. As for ettringite powder, carbonation is known to result in the formation of carbonates (vaterite and aragonite), alumina gel and gibbsite [36]. Figure 7 (f) shows the formation of carbonate crystals between the needles of ettringite with a shape that

resemble to vaterite (hexagonal) and calcite (orthorhombic) [46]. Indeed, XRD results (Table 3) confirm the formation of these two carbonates.

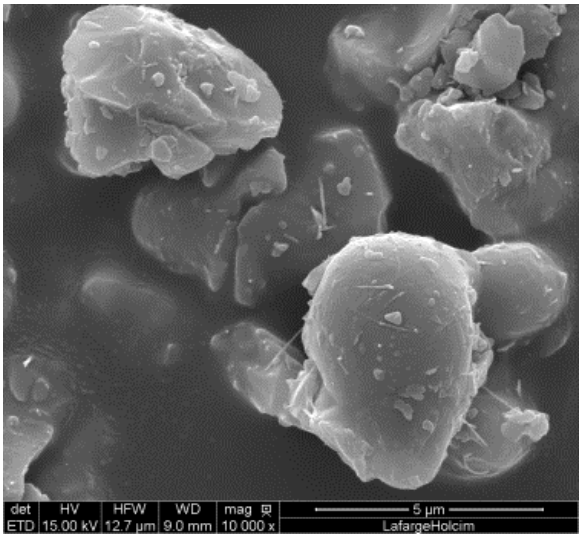

(a) C_3S before carbonation

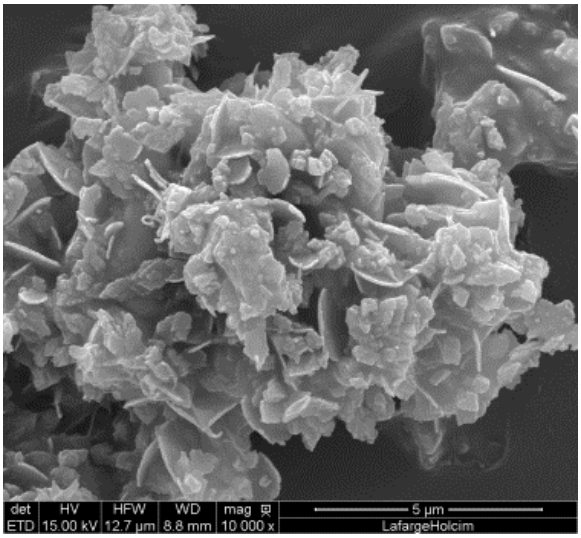

(b) C_3S carbonated at 93%

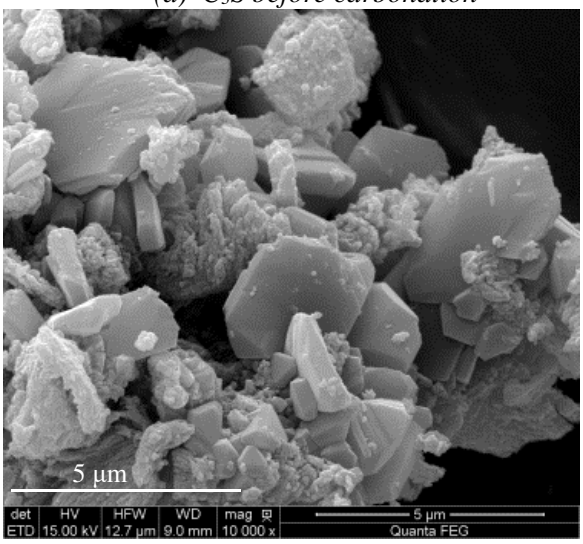

(c) CH before carbonation

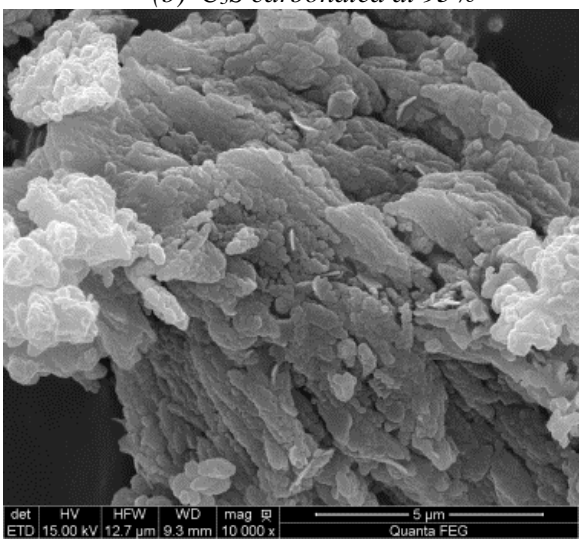

(d) CH carbonated at 93%

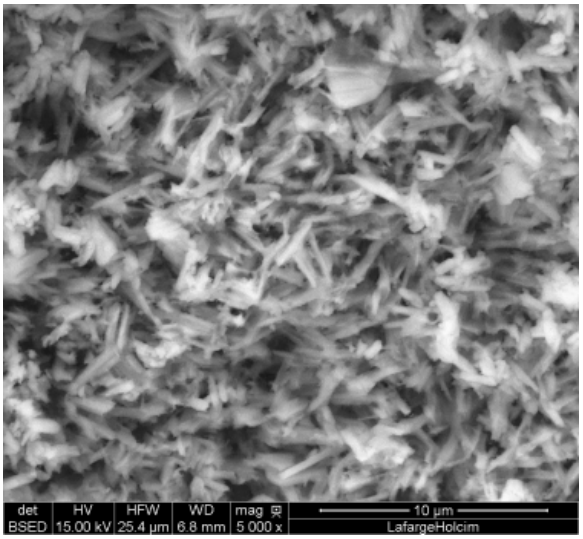

(e) Non-carbonated ettringite

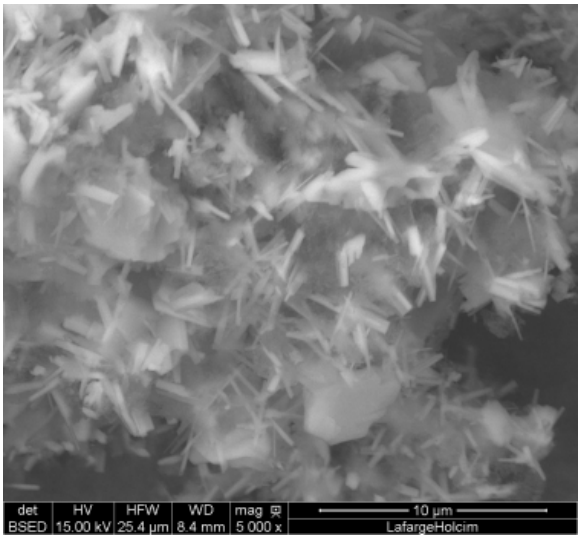

(f) Ettringite carbonated at 93% RH

Figure 7 : Morphological evolution of C_3S, CH and AFt powders before carbonation and after

exposure to carbonation at 93% RH

3.3 Reaction order analysis

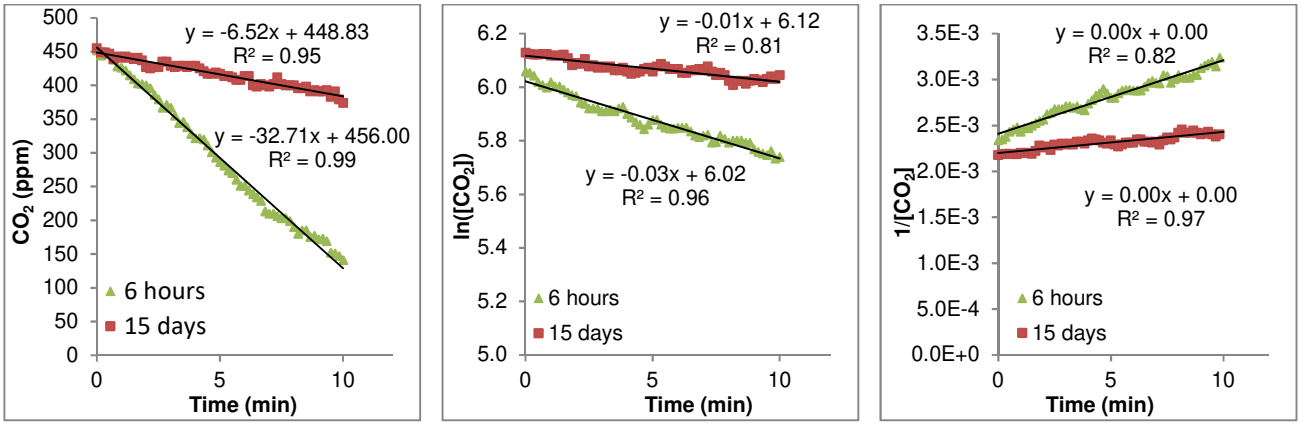

(a) **(b)** **(c)**

Figure 8: Reaction order analysis of portlandite after 6 hours and 15 days of exposure to carbonation. Order 0 (a), order 1 (b), order 2 (c)

Figure 8 shows an example of the reaction order analysis of portlandite powder carbonated at 33% RH. The analysis of Figure 8 reveals that the best linear fit for the considered timescale is obtained for the zeroth order (cf. Table 4). Consequently, the carbonation reaction kinetics (hence the CO_2 binding capacity) are independent of the CO_2 concentration within the concentration range of our experiments (450 ± 100 ppm). In agreement with these results, Van Balen et al. [47] and Shih et al. [20] suggest that the carbonation reaction of lime and portlandite powders at 7 - 17% CO_2 and 3.15-12.6% of CO_2, respectively, are of order 0.

Material	RH (%)	Exposure period (day)	order 0	order 1	order 2
CH	93	1	**0.98**	0.97	0.86
		8	**0.69**	0.62	0.68
	55	2	**0.98**	0.98	0.80
		13	**0.88**	0.80	0.81
	33	8 hours	**0.99**	0.96	0.96
		15	**0.85**	0.81	0.82
C-S-H	93	6 hours	**0.99**	0.99	0.98
		7	**0.92**	0.91	0.91
	55	5 hours	**0.99**	0.99	0.98
		22	**0.82**	0.81	0.82
	33	1	**0.99**	0.99	0.98
		22	**0.54**	0.51	0.53
AFt	93	1	**0.99**	0.97	0.96
		28	**0.91**	0.89	0.87
	55	8 hours	**0.96**	0.95	0.94

		17	0.91	**0.92**	0.89
	33	8 hours	**0.97**	0.83	0.83
		10	**0.67**	0.29	0.29
C_3S	93	4 hours	**0.95**	0.94	0.93
		9	**0.99**	0.99	0.97
	55	1	**0.99**	0.98	0.98
		12	0.78	0.78	**0.79**
	33	6 hours	**0.96**	0.95	0.94
		6	**0.42**	0.41	0.36
C_2S	93	1	0.96	**0.96**	0.96
		11	0.96	**0.97**	0.97
	55	0	0.96	0.96	**0.97**
		11	**0.92**	0.92	0.91
	33	2	**0.92**	0.92	0.92
		10	**0.84**	0.83	0.84
C_3A	93	2	**0.97**	0.97	0.91
		10	0.95	0.89	**0.96**
	55	0	**0.97**	0.96	0.97
		9	**0.57**	0.56	0.56
	33	0	**0.85**	0.85	0.85
		10	0.19	0.20	**0.21**

Table 4: R-square values for the reaction order analysis

Table 4 gives a summary of the reaction order analysis of the tested materials at different RH levels, and the R-squared of the linear fit analysis of the reaction orders. From analyzing the CO_2-uptake curves, it is noticed that the carbonation reaction during the first week of exposure is zeroth order in most cases. However, for anhydrous powders, a good fit is obtained for all orders. This result could be due to the carbonation reaction of more than one reactant. Still, Table 4 shows very comparable results of the fit quality of the CO_2-uptake curves for order 0, 1 and 2.

3.4 CO_2-binding capacity of anhydrous minerals from IBR

For each tested anhydrous material, Figure 9 and Figure 10 give the *IBR* and $B_{\_CO2}$, respectively. The *IBR* of anhydrous materials decreases with the exposure time. Note that since the *IBR* values are higher than the detection limit of the setup (5.8×10^{-10} $g_{co2}.g_{powder}^{-1}.s^{-1}$), these results refer to the properties of the materials rather than to any cell leakage. The *IBR* depends on the RH: the higher the RH, the higher the CO_2-binding rate. The *IBR* varies from [10^{-8} to 10^{-10}], [10^{-8} to 10^{-9}], and [10^{-7} to 10^{-9}] $g_{co2}.g_{powder}^{-1}.s^{-1}$ when the carbonation tests are carried out at 33% RH, 55% RH, and 93% RH, respectively. It is known that the controlling factor in the carbonation reaction rate is the dissolution of CaO and gaseous CO_2. At high RH, there is more water present to dissolve CaO and

CO_2, which increases the rate of the reaction. After 14 days of exposure to ambient CO_2 in climate chambers with constant RH levels (33, 55 and 93%), no anhydrous material reached the maximum binding capacity MBC, which was theoretically calculated (Table 2).

A slight carbonation of C_2S and C_3A powders was observed. The highest *CBC* was observed for C_3S powders carbonated at 93% RH. Furthermore, Figure 9.b shows that, after 14 days of exposure, the amount of bound CO_2 at 93% RH of the C_2S powder continued to increase but at a very slow rate ($2x10^{-9}$ $g_{CO2}.g_{powder}.s^{-1}$) while this rate was 10 times higher for C_3S powder.

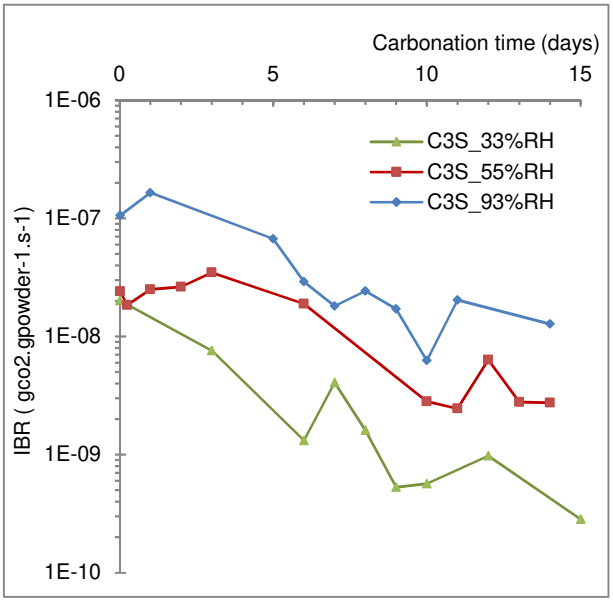

(a)

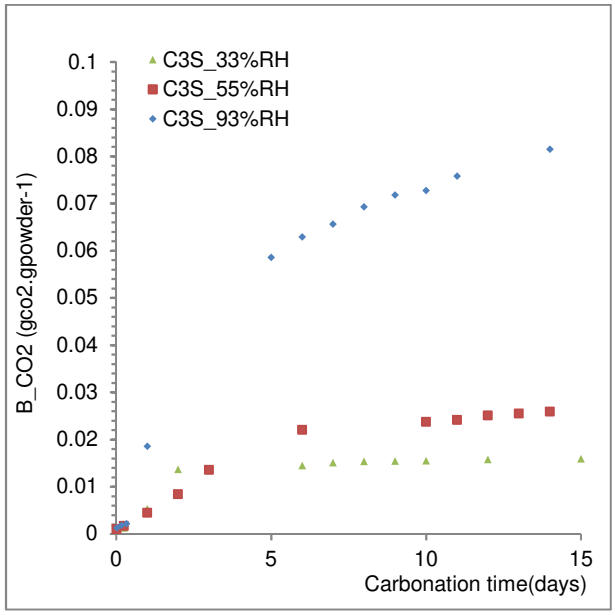

(a)

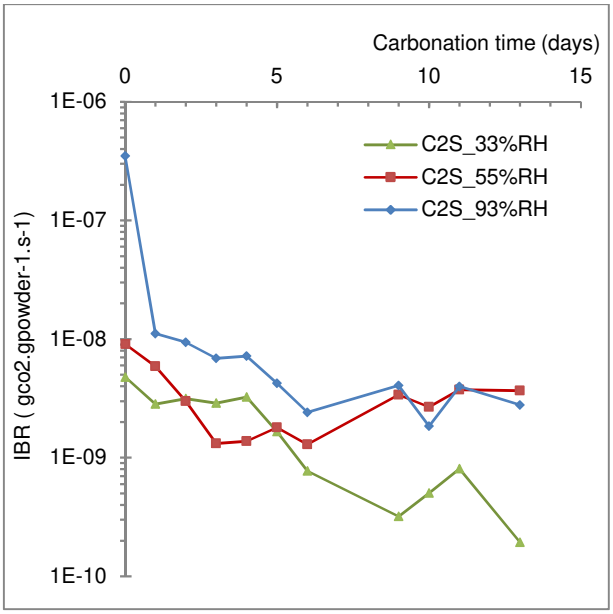

(b)

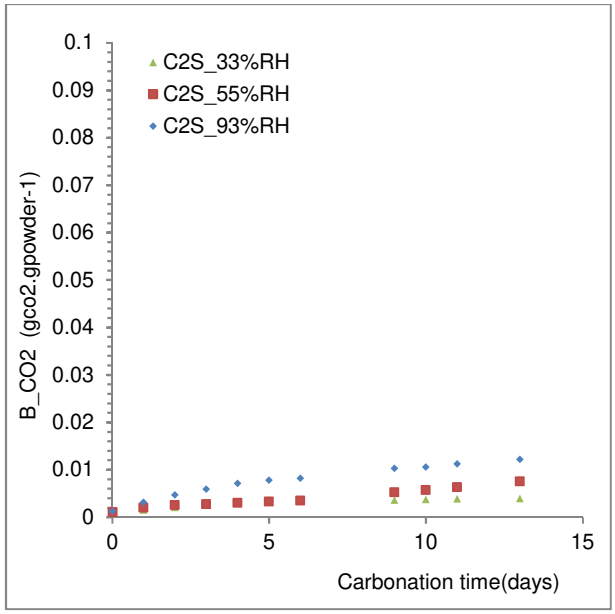

(b)

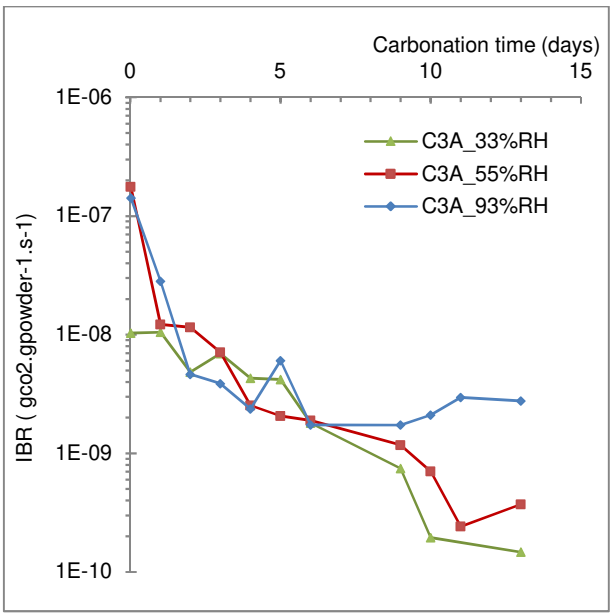

(c)

Figure 9: *IBR* of anhydrous phases

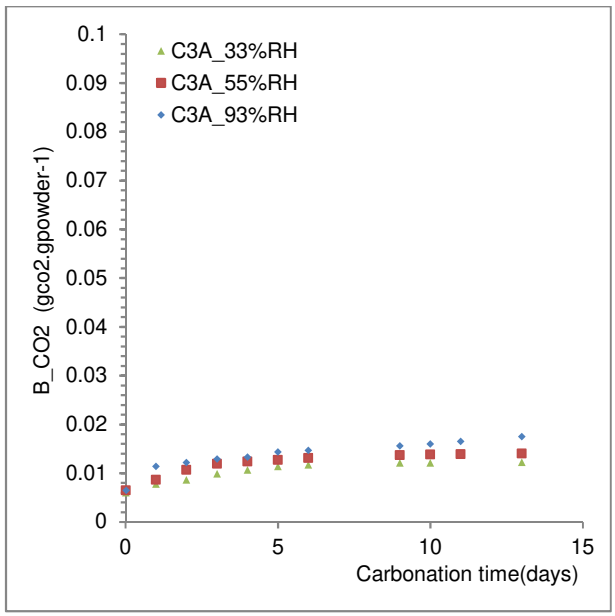

(c)

Figure 10: the amount of bound CO_2 at different carbonation periods of anhydrous phases

3.5 CO2-binding capacity of hydrates from IBR

For each tested hydrate, Figure 11 and Figure 12 give the *IBR* and $B_{\_CO2}$, respectively. Figure 11 (a) shows that the *IBR* of ettringite powder decreased by one order of magnitude only after 2 days of carbonation at 33% and 55% RH. At 55%, the *IBR* only slightly changed afterwards even after 29 days of carbonation, while the detection limit of the experimental setup was reached after 8 days of carbonation at 33% RH. Therefore, the experiments at these two RH levels were stopped after 11 and 28 days. Ettringite powder only slightly carbonates at 33% and 55% RH: *CBC* are $0.1.10^{-2}$ and 2.10^{-2} $g_{co2}.g_{powder}^{-1}$, respectively. On the other hand, at 93% RH, ettringite carbonated with a high *IBR* until 28 days of exposure, to reach a $B_{\_CO2}$ of 16.10^{-2} $g_{co2}.g_{powder}^{-1}$ that slightly varied afterwards. The present results confirm that the role of water in the carbonation of ettringite is highly important. It was also reported by Robl et al. [48] that ettringite only carbonates at 400 ppm CO_2 when ambient RH is higher than 60%.

Figure 11(b) shows that the *IBR* of portlandite decreased by 3 orders of magnitudes after 10 days of exposure to ambient CO_2 concentration at 93% and 55% RH. Consequently, Figure 12(b) shows that the $B_{\_CO2}$ increased significantly during the first 10 days of exposure to carbonation to reach a plateau that corresponds to its *CBC* afterwards (19.10^{-2} and 16.10^{-2} $g_{co2}.g_{powder}^{-1}$ at 93 and 55% RH

respectively). When carbonated at 33% RH, portlandite's *IBR* only decreased significantly after 16 days of carbonation to reach a *CBC* of 10.10^{-2} $g_{co2}.g_{powder}^{-1}$.

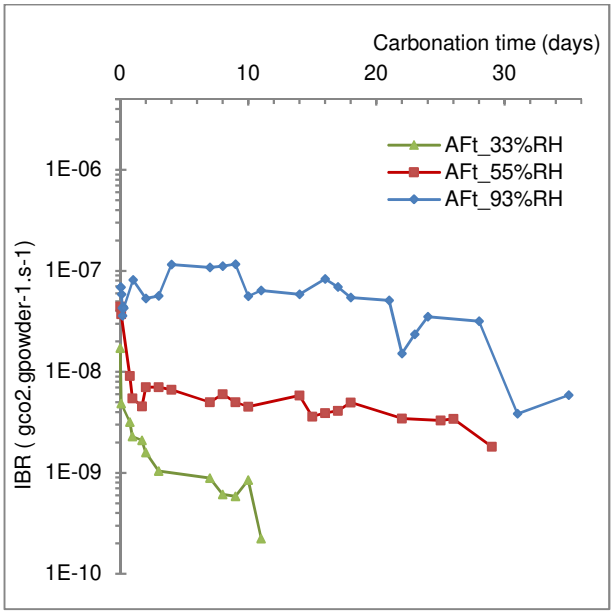

(a)

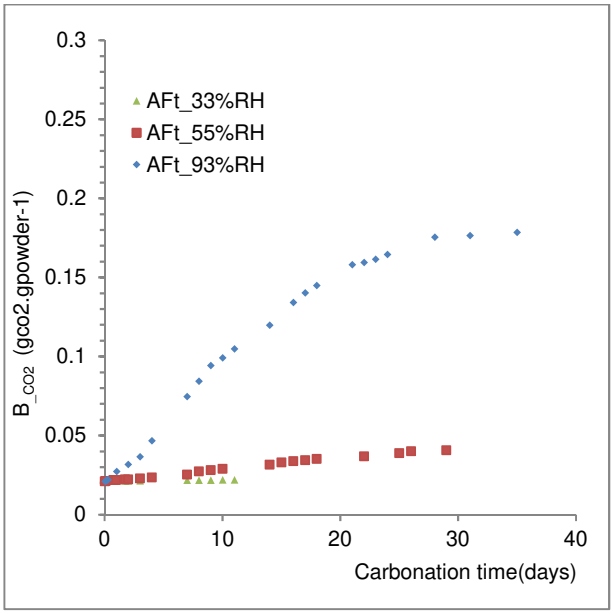

(a)

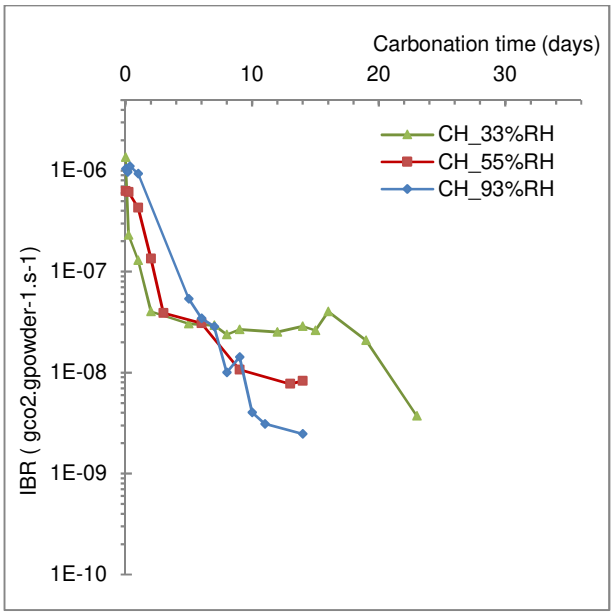

(b)

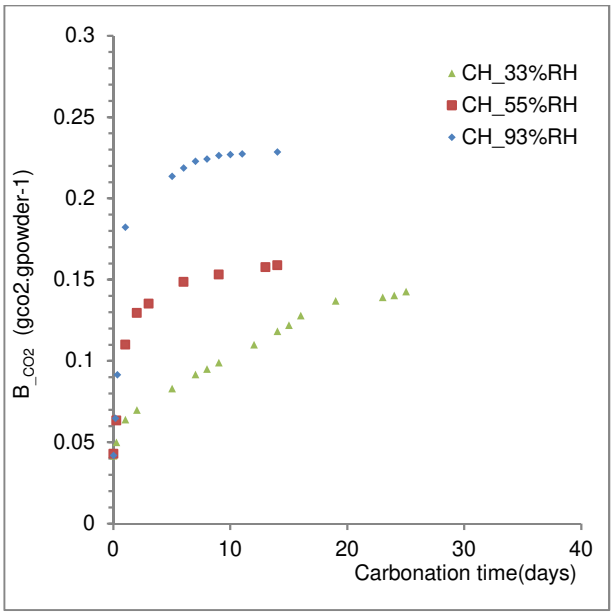

(b)

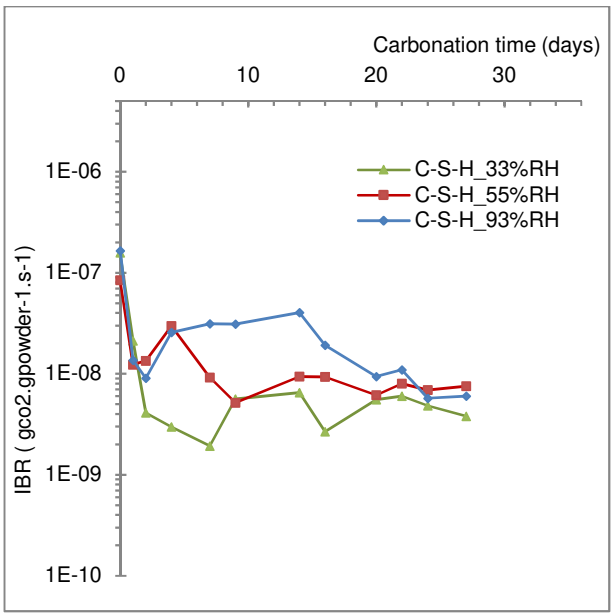

(c)

Figure 11: *IBR* of hydrates phases

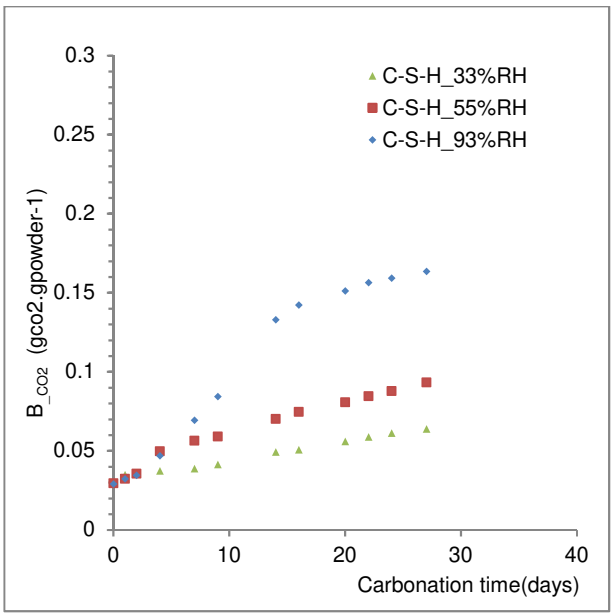

(c)

Figure 12: the amount of bound CO_2 at different carbonation periods of hydrates

As shown in Figure 11 (c), the *IBR* of the C-S-H powder decreased by almost one order of magnitude after two days of carbonation at 93% and 55% RH, 2 orders of magnitude at 33% RH after 9 days and only slightly varied afterwards. At three RH levels, the CBC of C-S-H powder was not reached, as observed in Figure 12 (c): the $B_{\_CO2}$ continues increasing even after 28 days of exposure to ambient carbon dioxide.

4 Discussion

4.1 Reaction vs. mass diffusion

In an attempt to identify the mass transport effect and the reactivity of the tested powders on a powder layer scale, the dimensionless Thiele modulus (Φ^2_n) was used to compare the transport and the reaction timescales. ϕ_n^2 is an important dimensionless number within the dual lens approach reaction, it appears in the mass balance, after introducing the dimensionless spatial variable [49].

$$\phi_n^2 = \frac{T_{diffusion}}{T_{reaction}} = \frac{d^2 * k_0 * \rho}{D_{e,CO2} * [CO2]_0} \qquad \text{Equation 9}$$

The Thiele modulus is defined as the ratio of the diffusion time ($T_{diffusion}$) to the reaction time ($T_{reaction}$). $D_{e,CO2}$ is the CO_2-effective diffusion coefficient in air (1.6×10^{-5} m²/s), $[CO_2]_0$ (g_{CO2}/m^3) is the CO_2 concentration at the surface of the grain, d(m) is the powder layer thickness, k_0 is the reaction

kinetic constant ($g_{CO2}.g^{-1}_{powder}.s^{-1}$) and ρ ($g_{powder}/m^3$) is the powder density. Low values of the Thiele modulus indicate surface reaction control and a significant amount of the CO_2 diffusing well into the grains' interior without reacting. High values of the Thiele modulus indicate that the surface reaction is rapid and that the reactant is consumed very close to the external surface so only very little penetrates into the interior of the grain [49].

	Highest reaction kinetic constant (10^{-6} $g_{CO2}.g^{-1}_{powder}.s^{-1}$)	Lowest reaction kinetic constant (10^{-10} $g_{CO2}.g^{-1}_{powder}.s^{-1}$)
Powder layer thickness (*d* in mm)	3	350

Table 5: The critical powder layer thickness at the lowest and highest values of the kintetic constant (Thiele modulus = 1)

The critical thickness of the powder layer is determined for a $\phi_n^2 = 1$ and the kinetic rate constant varies between 10^{-10} and 10^{-6} $g_{CO2}.g^{-1}_{powder}.s^{-1}$ (lowest and highest values determined from our experiments). For a powder layer of a thickness lower than 3 mm (which is the case in our study), the Thiele modulus is largely lower than 1. This result shows that the diffusion of CO_2 into the pores water is fast; so that the limiting factor is the CO_2 uptake by the solids.

4.2 *From instantaneous rate to "cumulative" CO_2 uptake*

The reliability of our test method results was investigated by comparing to the *CBC* values at the end of the carbonation period of each material obtained by both TGA and our method (cf. Table 2). Figure 13 shows that the *CBC* from TGA analysis and the CBC calculated based on our test method are in agreement. The difference between TGA and the developed test method are found to be evenly distributed along the mean trend: no evidence of an offset related with the mineral type, relative humidity or CBC range is observed. Nevertheless, it is worth noting that these values are not an average of repeated experiments, the latters were only performed once. Comparing average values would be more representative. These results are very promising regarding the accuracy and reliability of the new test method because they show that the analysis of the CO_2-uptake curves corresponds well to the carbonation reaction, since TGA data are hard evidence that the uptake of carbon dioxide is due to carbonation [19].

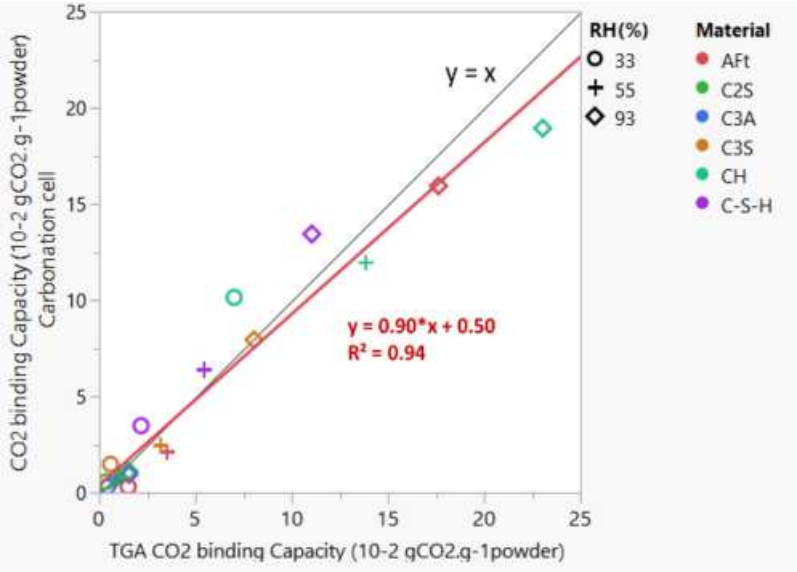

Figure 13: TGA CO_2-binding capacity vs. the carbonation cell CO_2-binding capacity (JMP)

The difference between TGA and the carbonation cell results could be a consequence of a slight carbonation during the preconditioning of the powders in the climate chamber even though soda lime was added. Moreover, the nature of these test methods is different: the *CBC* from TGA is determined purely on the basis of changes in the mass with respect to temperature and in correspondence with the amount of volatile matter and moisture content, and the carbonation cell test method is based on the measurement of the instantaneous CO_2 binding rate determined punctually during the carbonation period.

Note that the amount of bound CO_2 determined by the developed test method is dependent on the frequency of the CO_2-uptake measurements, especially during the first three days of exposure to ambient CO_2 concentration. The results reliability also depend on the response time and precision of the CO_2 gas sensor, especially for highly reactive phases.

The method developed to determine the CO_2 binding capacity and rate is simple, safe, reliable and cost-effective compared to thermogravimetric analysis. Results from this test method allow for the determination of the amount of bound CO_2 under different relative humidity levels, rather than predicting this value from C-S-H and CH content in the paste or CaO content in the cement. Moreover, the carbonation reaction kinetics can be determined at different periods of carbonation which is of high interest in the modeling of the carbonation front progress. The method is timesaving comparing to TGA as the latter requires approximately 2 hours depending on the heating rate, while a single CO_2-uptake measurement doesn't exceed 20 min. Nevertheless, TGA

analysis are important for this test method to determine the degree of carbonation after the preconditioning period in order to investigate the absolute total CO_2 content of the tested material. The test method can be improved by using a CO_2 sensor with lower response time, performing more measurements, which results in the improvement of integration method accuracy, and controlling the CO_2 concentration inside the room, especially for first and second order reactions. Nevertheless, the agreement between the results obtained from the two techniques is quite promising (Figure 13), since they differ by no more than 38% for the range of the conditions and materials tested.

4.3 Reaction mechanisms

4.3.1 Anhydrous carbonation

Regarding the carbonation of anhydrous materials, the *CBC* of C_2S and C_3A powders didn't exceed 2.10^{-2} $g_{CO2}.g^{-1}_{powder}$. However, C_3S powder carbonated significantly at 93% RH only (DoC = 14%). The previous work of Galan et al [13] also suggests that the minimum humidity needed to start the carbonation process is greater than 33% is needed.

Figure 6 shows a decrease in the density and a significant increase in the BET surface area of C_3S and C_2S powders due to carbonation, which can be explained by the formation of a thin layer of C-S-H on the surface of the grains [50][51]. Indeed, Houst et al. [52] reported that the carbonation of β-C_2S and C_3S results in the formation of aragonite, silica gel and a small amount of C-S-H, no trace of calcium hydroxide is observed during the carbonation [52].

The same result is observed for C_3A powder, which could be due to the formation of aluminum hydroxide since Figure 5 shows that the TGA results of C_3A powder after exposure to carbonation reveal a peak around 280-300°C, which corresponds to the decomposition of aluminum hydroxide.

The fact that only C_3S powder reacted at 93% RH could be explained by the high reactivity of C_3S with water, giving rise to the formation of calcium hydroxide and a number of different amorphous or poorly crystalline calcium silicate hydrates phases that would carbonate rapidly. These results are generally consistent with previous studies, which show that even though C_3A is much more water reactive than C_3S and C_2S [12], it only carbonates slowly.

4.3.2 Hydrates carbonation

The amount of bound CO_2 of both anhydrous and hydrates increased with the RH level where water is more available for the dissolution of CO_2 and CaO.

Although portlandite powder carbonated significantly at the three RH levels, the *CBC* is reached only after 7 days of carbonation. Images of portlandite powder shown in Figure 7 could explain the rapid decrease of the IBR, which would be due to the fact that the carbonation takes place on the surface of the grains, and its rate of proceeding inwards is very slow. Hence, when the surface is covered with $CaCO_3$, the carbonation is practically ceased. The same observation is drawn by Ashraf et al [14] regarding the accelerated carbonation of calcium silicate phases that occurs in two distinct stages: the first one is associated with a very rapid rate of carbonation, and the second is controlled by the diffusion in the carbonation products layer.

This is also facilitated by the relatively small surface areas of portlandite crystals in comparison with calcium silicate hydrates. This phenomenon is similar to the one addressed by Sohn and Szekeley [53] for porous solid pellets, where intragrain diffusion resistance may become so large that it will control the progress of the reaction process.

Moreover, Galan et al. [54] investigated the permeability of the $CaCO_3$ layer on the surface of portlandite and reported that this layer provides significant protection against diffusion of Ca^{2+} and OH^- ions, which hinders further carbonation. However, in the case of ettringite, which is a fibrous-form material, the carbonates could form between its needles (see Figure 7) which would not hinder the CO_2 diffusion nor the CaO dissolution. Indeed, Figure 12 shows that the *CBC* of ettringite is reached 18 days after portlandite's and the *IBR* remains constant for 20 days when ettringite is carbonated at 93% RH.

The carbonation of C-S-H is found to occur at a slower initial rate than the carbonation of CH because of the more rapid dissolution of CH [55][56]. This behavior reverses when the formation of microcrystalline $CaCO_3$ around reacting CH crystals inhibits further accessibility and slows down the portlandite dissolution, while the carbonation rate of C-S-H remains almost constant (very slow variation) even after 27 days of carbonation.

TGA and carbonation cell results show that the pure hydrates did not carbonate completely, their degree of carbonation did not exceed 45% in the present study (Table 2). In agreement with our results concerning portlandite's carbonation, Grandet [57] reported that the degree of carbonation

of portlandite is limited to 50-60%. Concerning the carbonation of pure ettringite, Castellote [58] found that ettringite carbonates up to 50% under 0.03% CO_2 and 3% CO_2, and carbonates completely at 10% CO_2.

4.4 Application of the results of this work

Results from this work would help to enhance the understanding of the kinetics of carbonation at high RH on the reactivity of clinker phases (C_3S, C_3A, C_4AF) during storage in silos or bags for long periods under different RH levels, which is an important issue for the industrial field.

The developed test method could be used to compare the CO_2 binding capacity of existing or innovative binders to assess their actual environmental benefits of CO_2 uptake by carbonation and investigate the life cycle assessment of cementitious materials after their preparation (in the case of precast concrete), during their service life, and after the end of the service life (recycled concrete) [59]. The NF P19-839, NF EN 16757 standards [59] state that the degree of carbonation of concrete strucures varies between 40% and 85% in a dry climate and under exposure to rain, respectively. However, our results in Table 2 reveal that even at 93% RH, the portlandite's degree of carbonation reached 39% only and the *IBR* varied very slightly after 7 days of carbonation. This suggests that higher RH or water content in addition to wetting drying cycle should be further investigated in terms of rate and maximum CO_2 uptake.

The results of this work could also improve the modeling of carbonation kinetics and the prediction of the shape of the carbonation front when the diffusion coefficient is also assessed. Since our results show that the CO_2-binding capacity of hydrates is reached after only 6 days (CH) or over 28 days (C-S-H) of exposure to carbonation, this means that the carbonation reaction could continue behind the carbonation depth determined by means of a pH indicator results, which means that the carbonation front shape is not completely sharp [5][55][60].

Carbonation is a physicochemical process controlled by the CO_2 binding capacity of the hardened cement paste and the diffusive transport of gaseous CO_2 through the cementitious materials' porous network. In order to study this phenomenon at the buiding product scale, results from the test method developed in this work should be completed with data on the gaseous CO_2 diffusion coefficient [8]

5 CONCLUSIONS

In the present work, a new test method is developed to determine the carbonation kinetics of the main synthetic phases present in the cement. Results allow us to draw the following conclusions:

- An original experimental setup was developed in order to measure the instantaneous CO_2 binding rate (IBR) and determine the amount of bound CO_2 during all periods of carbonation. The test method is advantageous because of its simplicity and cost-efficiency. Results from this test method agree with TGA results, which is promising regarding the accuracy and reliability of the test method. However, the test method could be improved by using sensors with lower response time and by increasing the frequency of the CO_2-uptake measurements to minimize the errors of the integration step.
- The controlling factor of the amount of bound CO_2 is the surface water-adsorbed, since the CO_2 binding capacity is found to increase with the RH under which carbonation tests were undertaken.
- Portlandite carbonates significantly compared to other hydrates, even at low RH, and the only carbonate formed is calcite. Ettringite carbonates remarkably at 93% RH (DoC=45%) and only slightly at 55% and 33% RH. Even though the carbonation rate of C-S-H is initially lower than that of portlandite, its carbonation continues with a constant rate even after 28 days of exposure, especially at 93% RH.
- No significant carbonation of the anhydrous materials was noticed. The actual amount of bound CO_2 was found to be lower than the theoretical maximum binding capacity calculated for all powders. Only at 93% RH, C_3S powders were carbonated (DoC=14%), which could be due to the formation of C-S-H as intermediate reaction product at this high RH level.
- The maximum degree of carbonation (DoC = 45%) was observed for ettringite powder, followed by portlandite (DoC = 38%) carbonated at 93% RH, which highlights the important contribution of these two hydrates in the carbonation performance of aluminous cements and Portland cements, respectively.

Funding

This work was funded by the National Association of Research and Technology (France) and the LafargeHolcim Innovation Center.

Acknowledgements

The authors would like to thank Dr. François Sorrentino for the synthesis of the tested materials, Cassandre Le Galliard, Didier Lapillonne and the analytical support team of the LafargeHolcim Innovation Center for their technical assistance. We also appreciate the helpful discussions with Prof. Heinz, Dr. Urbonas and Dr. Irbe.

No conflict of interest

The authors declare that they have no conflict of interest.

References

[1] V.G. Papadakis, C.G. Vayenas, M.N. Fardis, Experimental investigation and mathematical modeling of the concrete carbonation problem, Chem. Eng. Sci. 46 (1991) 1333–1338.

[2] W. Ashraf, Carbonation of cement-based materials: Challenges and opportunities, Constr. Build. Mater. 120 (2016) 558–570.

[3] L.J. Parrott, A review of carbonation in reinforced concrete, Cement and Concrete Association, Slough, England, 1987.

[4] Y.F. Houst, H. Folker, H. Wittmann, Depth profiles of carbonates fonned during natural carbonation, Cem. Concr. Res. (2002).

[5] P. Turcry, L. Oksri-Nelfia, A. Younsi, A. Aït-Mokhtar, Analysis of an accelerated carbonation test with severe preconditioning, Cem. Concr. Res. 57 (2014) 70–78.

[6] O. Omikrine Metalssi, A. Aït-Mokhtar, P. Turcry, A proposed modelling of coupling carbonation-porosity-moisture transfer in concrete based on mass balance equilibrium, Constr. Build. Mater. 230 (2020) 116997.

[7] V.G. Papadakis, C.G. Vayenas, M.N. Fardis, A reaction engineering approach to the problem of concrete carbonation, AIChE J. 35 (1989) 1639–1650.

[8] M. Boumaaza, B. Huet, G. Pham, P. Turcry, A. Aït-Mokhtar, C. Gehlen, A new test method to determine the gaseous oxygen diffusion coefficient of cement pastes as a function of hydration duration, microstructure, and relative humidity, Mater. Struct. 51 (2018).

[9] M. Boumaaza, B. Huet, P. Turcry, C. Gehlen, A. Aït-Mokhtar, D. Heinz, Gas diffusivity test method development: Effect of cement paste saturation degree and concrete specimen thickness, Proc. 12th Fib Int. PhD Symp. Civ. Eng. (2018) 1087–1094.

[10] C.D. Lawrence, Transport of Oxygen Through Concrete., Br. Ceram. Proc. (1984) 277–293.

[11] D. Benavente, C. Pla, Effect of pore structure and moisture content on gas diffusion and permeability in porous building stones, Mater. Struct. Constr. 51 (2018) 1–14.

[12] J. Sun, Carbonation kinetics of cementitious materials used in the geological disposal of radioactive waste, University College London, 2010.

[13] I. Galan, C. Andrade, M. Castellote, Natural and accelerated CO2 binding kinetics in cement paste at different relative humidities, Cem. Concr. Res. 49 (2013) 21–28.

[14] W. Ashraf, J. Olek, Carbonation activated binders from pure calcium silicates: Reaction kinetics and performance controlling factors, Cem. Concr. Compos. 93 (2018) 85–98.

[15] N.C. Collier, Transition and decomposition temperatures of cement phases - a collection of thermal analysis data, Ceram. - Silikaty. 60 (2016) 338–343.

[16] G. Villain, M. Thiery, G. Platret, Measurement methods of carbonation profiles in concrete: Thermogravimetry, chemical analysis and gammadensimetry, Cem. Concr. Res. 37 (2007) 1182–1192.

[17] B. Wu, G. Ye, Study of carbonation rate of synthetic C-S-H by XRD, NMR and FTIR, Heron. 64 (2019) 21–38.

[18] R. Ylmén, U. Jäglid, Carbonation of Portland Cement Studied by Diffuse Reflection Fourier Transform Infrared Spectroscopy, Int. J. Concr. Struct. Mater. 7 (2013) 119–125.

[19] K. Van Balen, Carbonation reaction of lime, kinetics at ambient temperature, Cem. Concr. Res. 35 (2005) 647–657.

[20] S.-M. Shih, C.-S. Ho, Y.-S. Song, J.-P. Lin, Kinetics of the Reaction of Ca(OH) 2 with CO 2 at Low Temperature, Ind. Eng. Chem. Res. 38 (2002) 1316–1322.

[21] A. El-Turki, M.A. Carter, M.A. Wilson, R.J. Ball, G.C. Allen, A microbalance study of the effects of hydraulicity and sand grain size on carbonation of lime and cement, Constr. Build. Mater. 23 (2009) 1423–1428.

[22] V. Nikulshina, M.E. Gálvez, A. Steinfeld, Kinetic analysis of the carbonation reactions for the capture of CO2 from air via the Ca(OH)2-CaCO3-CaO solar thermochemical cycle, Chem. Eng. J. 129 (2007) 75–83.

[23] T.AONO, Studies on the reactions between gas and solid, part II, absorption of CO2 by CaO and Ca(OH)2, Bull. Chem. Soc. Jpn. 6 (1931) 319–324.

[24] F. Sorrentino, Upscaling the synthesis of tricalcium silicate and alite, Cem. Wapno Bet. 8 (2008) 177–183.

[25] A. Morandeau, M. Thiéry, P. Dangla, Investigation of the carbonation mechanism of CH and C-S-H in terms of kinetics, microstructure changes and moisture properties, Cem. Concr. Res. 56 (2014) 153–170.

[26] M. Balonis, F.P. Glasser, The density of cement phases, Cem. Concr. Res. 39 (2009) 733–739.

[27] P. López-Arce, L.S. Gómez-Villalba, S. Martínez-Ramírez, M. Álvarez de Buergo, R. Fort, Influence of relative humidity on the carbonation of calcium hydroxide nanoparticles and the formation of calcium carbonate polymorphs, Powder Technol. 205 (2011) 263–269.

[28] H.F.W. Taylor, Cement Chemistry, 2nd ed, Thomas Telford Publishing, 1997.

[29] T. Nishikawa, K. Suzuki, S. Ito, Decomposition of synthesized ettringite by carbonation, Cem. Concr. Res. 22 (1992) 6–14.

[30] J. Plank, M. Zhang-Preße, N.P. Ivleva, R. Niessner, Stability of single phase C3A hydrates against pressurized CO2, Constr. Build. Mater. 122 (2016) 426–434.

[31] E. Brunauer, Stephen; Emmett, P. H.; Teller, Adsorption of Gases in Multimolecular Layers, J. Am. Chem. Soc. (1938) 309–319.

[32] D. Helsel, M. A., Ferraris, C. F., and Bentz, Comparative study of methods to measure the density of Cementious powders, J. Test. Eval. 44 (2016) 2147–2154.

[33] S. Meulenyzer, J. Chanussot, J.J. Chen, S. Crombez, Spectral-spatial image processing strategies for classifying multispectral SEM-EDS X-Ray maps of cementitious materials, 14th Euroseminar Microsc. Appl. to Build. Mater. (2013).

[34] R.J. Flatt, G.W. Scherer, J.W. Bullard, Why alite stops hydrating below 80% relative humidity, Cem. Concr. Res. 41 (2011) 987–992.

[35] O. Regnault, V. Lagneau, H. Schneider, Experimental measurement of portlandite carbonation kinetics with supercritical CO2, Chem. Geol. 265 (2009) 113–121.

[36] I. Galan, F.P. Glasser, D. Baza, C. Andrade, Assessment of the protective effect of carbonation on portlandite crystals, Cem. Concr. Res. 74 (2015) 68–77.

[37] L. Black, K. Garbev, I. Gee, Surface carbonation of synthetic C-S-H samples: A comparison

between fresh and aged C-S-H using X-ray photoelectron spectroscopy, Cem. Concr. Res. (2008).

[38] L. Black, K. Garbev, G. Beuchle, P. Stemmermann, D. Schild, X-ray photoelectron spectroscopic investigation of nanocrystalline calcium silicate hydrates synthesised by reactive milling, Cem. Concr. Res. 36 (2006) 1023–1031.

[39] R. B. Perkins, C. Palmer D., Solubility of ettringite, Geochim. Cosmochim. Acta. 63 (1999) 1969–1980.

[40] Q. Zhou, F.P. Glasser, Kinetics and mechanism of the carbonation of ettringite, Adv. Cem. Res. 12 (2000) 131–136.

[41] S. Goto, K. Suenaga, T. Kado, M. Fukuhara, Calcium Silicate Carbonation Products, J. Am. Ceram. Soc. 78 (1995) 2867–2872.

[42] V. Rostami, Y. Shao, A.J. Boyd, Z. He, Microstructure of cement paste subject to early carbonation curing, Cem. Concr. Res. (2012).

[43] O. Shtepenko, C. Hills, A. Brough, M. Thomas, The effect of carbon dioxide on beta-dicalcium silicate and Portland cement, Chem. Eng. J. 118 (2006) 107–118.

[44] W. Ashraf, J. Olek, Elucidating the accelerated carbonation products of calcium silicates using multi-technique approach, J. CO2 Util. 23 (2018) 61–74.

[45] J. De Han, G.H. Pan, W. Sun, C.H. Wang, D. Cui, Application of nanoindentation to investigate chemomechanical properties change of cement paste in the carbonation reaction, Sci. China Technol. Sci. 55 (2012) 616–622.

[46] E. Hamza, Contribution a l'etude des eaux geothermales du sud tunisien : etude des mecanismes et de la prevention des phenomenes d'entartrage, L'Institut National des Sciences Appliquées de Toulouse, 1999.

[47] M. Nedeljković, B. Ghiassi, S. Melzer, C. Kooij, S. van der Laan, G. Ye, CO2 binding capacity of alkali-activated fly ash and slag pastes, Ceram. Int. 44 (2018) 19646–19660.

[48] T.L. Robl, U.M. Graham, D.N. Taulbee, W. Giles, The effect of carbonation reactions on the long term stability of products made from dry FGD materials, ACS Div. Fuel Chem. (1996).

[49] H. Scott Fogler, Elements of chemical reaction engineering, Chem. Eng. Sci. 42 (1987) 2493.

[50] J.F. YOUNG, R.L. BERGER, J. BREESE, Accelerated Curing of Compacted Calcium Silicate Mortars on Exposure to CO2, J. Am. Ceram. Soc. 57 (1974) 394–397.

[51] D. Wang, Y. Fang, Y. Zhang, J. Chang, Changes in mineral composition, growth of calcite crystal, and promotion of physico-chemical properties induced by carbonation of β-C2S, J. CO2 Util. 34 (2019) 149–162.

[52] Y.F. Houst, Diffusion de gaz, carbonatation et retrait de la pate de ciment durcie, Ecole polytechnique federale de Lausanne, 1992.

[53] H.Y. Sohn, J. Szekely, The effect of intragrain diffusion on the reaction between a porous solid and a gas, Chem. Eng. Sci. 29 (1974) 630–634.

[54] I. Galan, C. Andrade, P. Mora, M.A. Sanjuan, Sequestration of CO2 by concrete carbonation, Environ. Sci. Technol. 44 (2010) 3181–3186.

[55] M. Thiery, G. Villain, P. Dangla, G. Platret, Investigation of the carbonation front shape on cementitious materials: Effects of the chemical kinetics, Cem. Concr. Res. 37 (2007) 1047–1058.

[56] I.G. Richardson, G.W. Groves, A.R. Brough, C.M. Dobson, The carbonation of OPC and OPC/silica fume hardened cement pastes in air under conditions of fixed humidity, Adv. Cem. Res. 5 (1993) 81–86.

[57] J. Grandet, Contribution à l'étude de la prise et de la carbonatation des mortiers au contact des matériaux poreux, Université Toulouse III, 1975.

[58] M. Castellote, L. Fernandez, C. Andrade, C. Alonso, Chemical changes and phase analysis of OPC pastes carbonated at different CO2 concentrations, Mater. Struct. 42 (2009) 515–525.

[59] Association Française de Normalisation (AFNOR), Nf P19-839, Nf En 16757, (2017).

[60] L.J. Parrott, D.C. Killoh, Carbonation in a 36 year old, in-situ concrete, Cem. Concr. Res. 19 (1989) 649–656.